Band Tail Engineering in Kesterite $Cu_2ZnSn(S,Se)_4$ Thin-Film Solar Cells with 11.8% Efficiency

Myeng Gil Gang[a,†], Seung Wook Shin[b,†], Mahesh P. Suryawanshi[a], Uma V. Ghorpade[a], Zhaoning Song[b], Jun Sung Jang[a], Jae Ho Yun[c], Yanfa Yan[b,], Jin Hyeok Kim[a,*]*

[a]*Optoelectronics Convergence Research Center and Department of Materials Science and Engineering, Chonnam National University, 300, Yongbong-Dong, Buk-Gu, Gwangju 61186, South Korea*

[b]*Department of Physics and Astronomy and Wright Center for photovoltaic Innovation and Commercialization, University of Toledo, Toledo, Ohio, 43606, United States*

[c]*Photovoltaic Laboratory, Korea Institute of Energy Research, 71-2, Jang-Dong, Yuesong-Gu, Daejeon 34129, South Korea*

AUTHOR INFORMATION

Corresponding Authors

[*]E-mail: yanfa.yan@utoledo.edu (Y. Yan)

[*]E-mail: jinhyeok@chonnam.ac.kr (J.H. Kim)

Author Contributions

[†]M. G. Gang and S. W. Shin contributed equally to this work

ABSTRACT

The efficiency of current kesterite $Cu_2ZnSn(S_x,Se_{1-x})_4$ (CZTSSe) thin-film solar cells is limited by the large open-circuit voltage (V_{oc}) deficit, which is associated with band tailing in CZTSSe. Herein, we report a facile process, *i.e.*, controlling the initial chamber pressure during the post-deposition annealing, to effectively lower the band tail states in the synthesized CZTSSe thin films. Through a detailed analysis of the external quantum efficiency derivative (dEQE/$d\lambda$) and low temperature photoluminescence (LTPL) data, we find that the band tail states are significantly influenced by the initial annealing pressure. After carefully optimizing the deposition processes and device design, we are able to synthesize kesterite CZTSSe thin films with energy differences between inflection of dEQE/$d\lambda$ and LTPL as small as 10 meV. These kesterite CZTSSe thin films enable the fabrication of solar cells with a champion efficiency of 11.8% with a low V_{oc} deficit of 582 mV. The results suggest that controlling annealing process is an effective approach to reduce the band tail in kesterite CZTSSe thin films.

Metal chalcogenide thin film solar cells (TFSCs) hold a great potential for producing clean and affordable solar electricity because they offer exceptional opportunities for low cost manufacturing of high performance photovoltaic (PV) modules.[1-6] In particular, $Cu(In,Ga)Se_2$ (CIGS) and CdTe TFSCs have already achieved high power conversion efficiencies (PCEs) over 22% and have shown steady growth in the renewable energy market.[1-2, 7] In spite of the outstanding performances, the widespread deployment of CIGS and CdTe TFSCs is hindered by the inclusion of rare (e.g., In, Ga, and Te) and environmentally unfriendly (*e.g.*, Cd) elements in the absorber materials.[8-9] The recently emerging kesterite-based absorber materials, such as Cu_2ZnSnS_4 (CZTS),

$Cu_2ZnSnSe_4$ (CZTSe), and $Cu_2ZnSn(S_x,Se_{1-x})_4$ (CZTSSe), have attracted significant attention due to their low toxicity and earth-abundant elemental constitutions, direct and tunable bandgaps from 1.0 to 1.5 eV, high absorption coefficients of 10^4 cm^{-1}, and high theoretical efficiencies of up to 30%.[2, 10-13] The record PCE of CZTSSe-based TFSCs has been steadily increased to 12.6% in 2014[2], but the progress has stalled in recent years.

Despite their similarities, CZTSSe TFSCs significantly underperform their sister technology CIGS TFSCs.[7] One of the main reason limiting the performance of CZTSSe is the large open-circuit voltage (V_{oc})-deficit, defined as E_g/q-V_{oc}, where E_g is bandgap energy of the kesterite absorber and q is the electron charge.[14-16] The V_{oc} deficit of the champion CZTSSe TFSCs (617 mV)[2] is significantly larger than that of their CIGS counterparts (310 mV).[7] Many studies attribute this deficit to band tailing caused by the cationic disordering.[14, 16-18] The natural complexity of the quaternary compounds increases the likelihood of formation of various defects, especially the anti-site defect complexes, which are believed to be the primary cause for the band tailing because of their low defect formation energies.[14, 19] These defects are likely formed during the high temperature sulfurization (or selenization) process which promotes a random distribution of cations in the crystal lattice, leading to the cationic disordering.[20] To reduce the V_{oc}-deficits of CZTSSe based TFSCs, recent efforts have focused on identification and control of band tail states in kesterite CZTSSe (see details in Table S1).[5, 10, 12, 15, 17, 21-34] Among various approach, one prospective pathway to mitigate band tailing is to develop a better control of the CZTSSe synthesized process conditions, most importantly, the post-deposition annealing conditions to suppress or remove cation site disorder and associated band tailing.

In this letter, we examine the interplay between the post-deposition annealing conditions and the band tailing in the CZTSSe films by a systematic investigation of the dependence of

CZTSSe thin film properties on annealing pressures and a detailed comparison of the energy difference between the inflection of external quantum efficiency derivative (dEQE)/$d\lambda$) and low temperature photoluminescence (LTPL) for the corresponding CZTSSe TFSCs. We show that band tail states in CZTSSe can be manipulated through a facile control of the initial chamber pressure during the annealing process. With careful optimization of all component layers, we achieve the champion CZTSSe TFSCs with a certificated PCE of 11.8%, a low V_{oc} deficit of 582 mV, and the smallest value of energy difference between dEQE/$d\lambda$ and LTPL (10 meV) measured under an AM 1.5G illumination.

Our CZTSSe thin films are obtained by annealing sputtered and soft-annealed Zn/Sn/Cu metallic precursors under a mixed S and Se vapor atmosphere as shown in Figure S1. Briefly, (i) a metallic precursor with stacking order of Cu/Sn/Zn was deposited on Mo coated soda lime glass (SLG) substrates at 0 ºC by sputtering; (ii) the metallic precursor was annealed at 300 ºC for 60 min under Ar atmosphere (i.e., `soft-annealing process`) to obtain Cu-Zn and Cu-Sn alloys with smooth morphologies; (iii) the soft-annealed precursor and chalcogen powders were placed in a graphite box (with a volume of ~ 406 cm^3) in a rapid thermal annealing (RTA) chamber; (iv) the chamber was evacuated to a base pressure of 1.0 x 10^{-3} Torr and then the initial pressure was controlled at 400, 500, 600, and 700 Torr through controlling the amount of Ar gas added to the chamber; (v) the chamber was heated up at a ramp rate of 10 ºC/s to 520 ºC and held isothermal for 10 min; (vi) the annealed film was naturally cooled for 1 hour. The detailed pressure and temperature profiles during the annealing process are shown in Figure S2 and S3. Experimental details are provided in the Supporting Information.

We first investigate the impacts of initial chamber pressure on the formation of kesterite CZTSSe by characterizing the structural, morphological, and compositional properties of CZTSSe films annealed under differnet pressures. Figure 1a shows X-ray diffraction (XRD) patterns of CZTSSe thin films annealed under different initial chamber pressures. All CZTSSe films show similar XRD patterns of three intense

diffraction peaks near 27.3˚, 45.2˚, and 53.7˚, corresponding to the (112), (220), and (312) planes, along with three minor peaks (17.5 ˚, 36.4 ˚ and 66.0 ˚) of the CZTSe kesterite structure. The peaks belonging to the CZTS kesterite phase also presents in the vicinity of the CZTSe peaks with higher diffraction angles due to smaller ionic radius of S^{2-} (0.184 nm) than Se^{2-} (0.198 nm).[3] However, it is known that distinguishing the kesterite CZTS phase by analyzing XRD patterns from secondary phases, such as tetragonal or cubic Cu_2SnS_3 (CTS) and cubic ZnS is difficult because their lattice constants are nearly identical. One promising solution for phase classification in CZTSSe thin films is Raman spectroscopy measurements with different excitation laser sources because Zn(S,Se) and $Cu_2Sn(S,Se)_3$ phases can be distinguished using 325 and 633 nm excitation laser sources, respectively (Figure S4).[3] From three Raman spectra using different excitation laser sources, no other phases are identified, indicating the formation of phase pure CZTSSe kesterite under all annealing conditions.

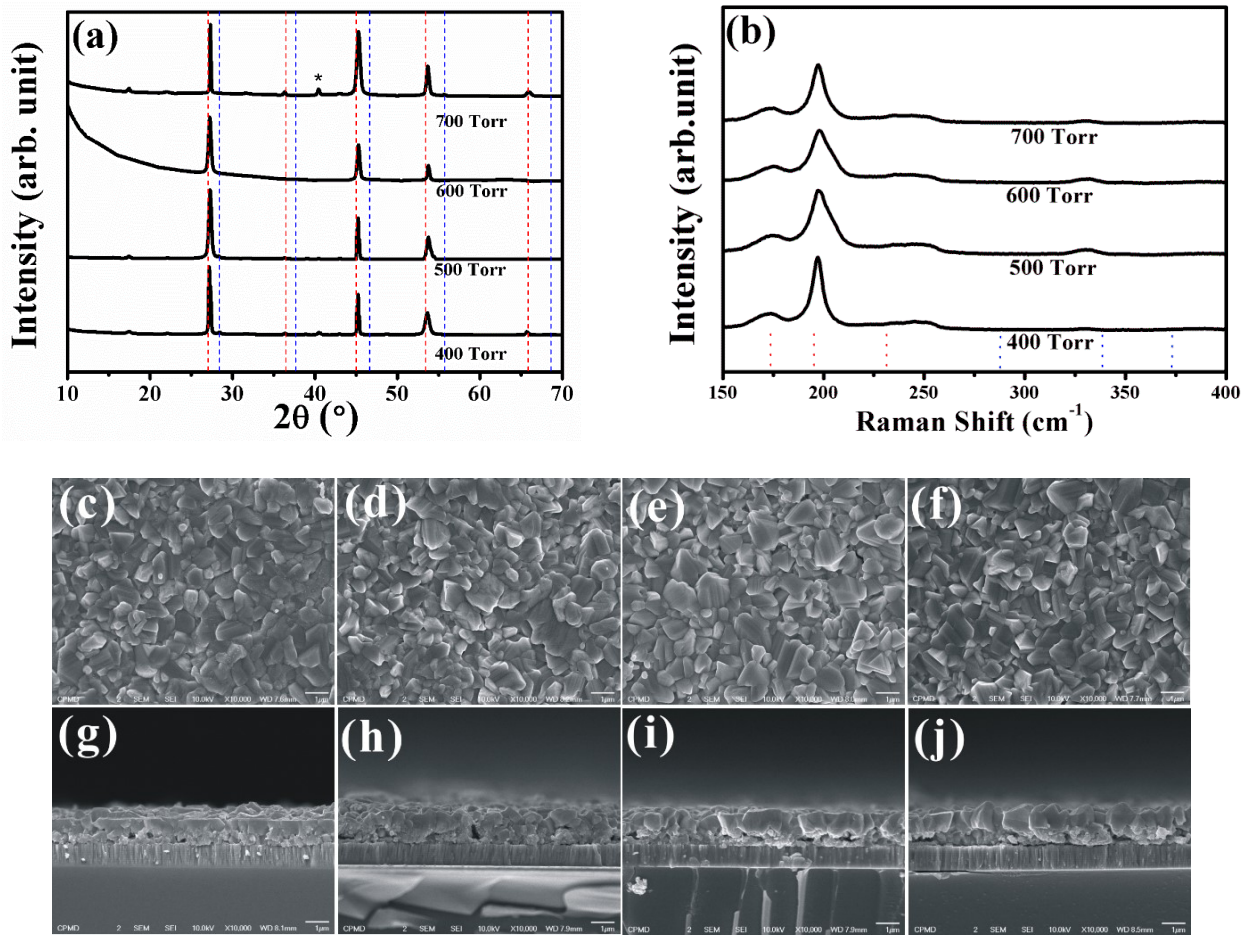

Figure 1. (a) X-ray diffraction patterns and (b) Raman spectra using 514 nm exitation laser source of CZTSSe thin films annealed under different initial chamber pressures. Red and blue dash lines in (a) and (b) indicate peaks for $Cu_2ZnSnSe_4$ and Cu_2ZnSnS_4, respectively. Surface- and cross-sectional SEM images of CZTSSe thin films annealed under the initial chamber pressure of (c, g) 400, (d, h) 500, (e, i) 600, and (f, j) 700 Torr, respectively.

Figure 1c-f shows surface scanning electron microscopy (SEM) images of CZTSSe films annealed under different pressures. All the films show smooth and dense morphology with grain size ranging from 0.5 to 1.5 μm. There is no significant difference regardless of initial chamber pressure. The cross-sectional SEM images (Figure 1g-j) reveal simililar bi-layered microstructures in all the films, consisting of more compact submicron sized grains on the top and smaller sized grains accompanied with voids at the bottom region. In particular, the thickness of the top layer increases with increasing annealing pressure. Additionally, the formation of interfacial $Mo(S,Se)_2$ layer between CZTSSe and Mo back contact is not observed, indicating a negligible thickness of less than 20 nm which is undetectable by SEM. Transmission electron microscopy (TEM) image (Figure S5) confirms that the interface between CZTSSe and Mo back contact layer is less than 20 nm. The Se/(S+Se) ratios for CZTSSe thin films as a function of initial chamber pressure measured using X-ray fluorescence (XRF) and inductively coupled plasma mass spectrometry (ICP-MS) characterizations as well as predicted from XRD and Raman spectra are shown in Table S2. The results show that Se/(S+Se) ratio in the film is strongly dependent on the initial chamber pressure. The measured and predicted Se/(S+Se) ratio slightly increases from 0.89 to 0.92~0.94 with increasing initial chamber pressure, likely due to the different equilibrium partial pressures of S and Se gases during the annealing process. The results suggest that S becomes more reactive with increasing initial chamber pressure.

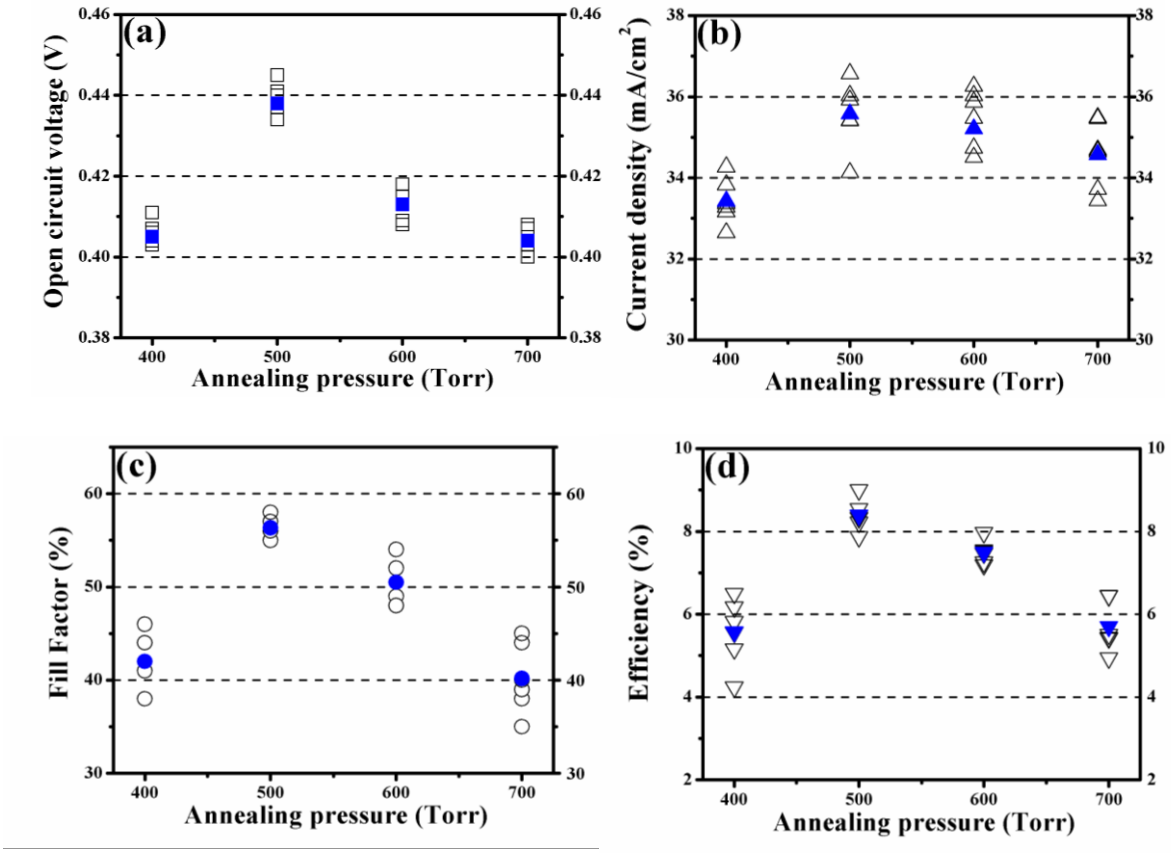

Figure 2. Device performance parameters of the CZTSSe TFSCs annealed under different initial chamber pressures, including (a) V_{oc}, (b) J_{sc}, (c) *FF*, and (d) η, measured under simulated AM 1.5G illumination. Each data set was obtained from 6 solar cells. Blue symbols show average values.

To further investigate the influence of annealing pressure on solar cell performance, we fabricated TFSCs using CZTSSe films annealed under different initial chamber pressures. Figure 2 shows the distribution of PV performance parameters of these devices, and the representative current-voltage (*J-V*) curves are shown in Figure S6a. The average and best performances of CZTSSe TFSCs increase when initial chamber pressure is increased from 400 to 500 Torr and then decrease when the pressure is further increased. Interestingly, the initial chamber pressure has larger impacts on V_{oc} and *FF* than on J_{sc} (See Table S3 for details). The smallest V_{oc}-deficit of 609 mV is achieved in CZTSSe TFSCs annealed under an initial chamber pressure of 500 Torr, while other devices show the V_{oc}-deficit values of over 670 mV.

To understand the relationship between V_{oc}-deficit caused by band tail states and performance of CZTSSe TFSCs as a function of initial chamber pressure, we compare the energy differences between the effective bandgap measured from the inflection of EQE, i.e., the peak in dEQE/$d\lambda$, and the bandgap measured from LTPL spectra (Figure 3). For all the CZTSSe samples, LTPL peaks are shifted to lower energies relative to the bandgaps determined by the EQE spectra. The energy differences determined from the dEQE/$d\lambda$ and LTPL data are 110, 27, 38, and 42 meV for the device with CZTSSe films annealed under the initial pressure of 400, 500, 600, and 700 Torr, respectively, showing the trend consistent with the variation of PV performance, especially the V_{OC} in CZTSSe TFSCs (Figure 2a). The large energy difference between bandgaps measured from dEQE/$d\lambda$ and LTPL is mainly attributed to antisite defect complexes in the CZTSSe layers, such as V_{cu}+ Sn_{Zn} and Cu_{Zn}+Sn_{Zn}, which introduce nonradiative recombination centers or band tailing.[2, 16, 26, 32] Additionally, notable differences are observed in the subbandgap absorption of these CZTSSe films, determined by the EQE data followed a reported method (Figure S7).[14] The 500 Torr sample exhibits the lowest subbandgap absorption coefficient, indicating the lowest band tail state density among the samples. The combined results suggest that precise control of the initial chamber pressure can effectively reduce the band tailing in the CZTSSe films and enhance device performance of CZTSSe TFSCs.

The underlying mechanisms for lower band tail states at higher initial chamber pressures are yet to be determined. Some possible hypotheses include (i) the high external pressure may reduce Sn loss and, consequently, reduce Sn-related antisite defects such as V_{Sn} and Zn_{Sn}; (ii) the high initial chamber pressure may enhance the Se contents near surface region, leading to less anitsite defect density than that with a lower Se content. We are undergoing investigations on different experimental conditions, such as substitution of Ag at Cu site, metal stacking order of the precursor, soft-annealing process (i.e., holding time, temperature, and atmosphere), and sulfo-selenization process (i.e., hold time, step annealing process, temperature, and etc.) for CZTSSe thin films, by using various characterization techniques to clearly explain the relationship between the initial chamber pressure and the reduced band tails.

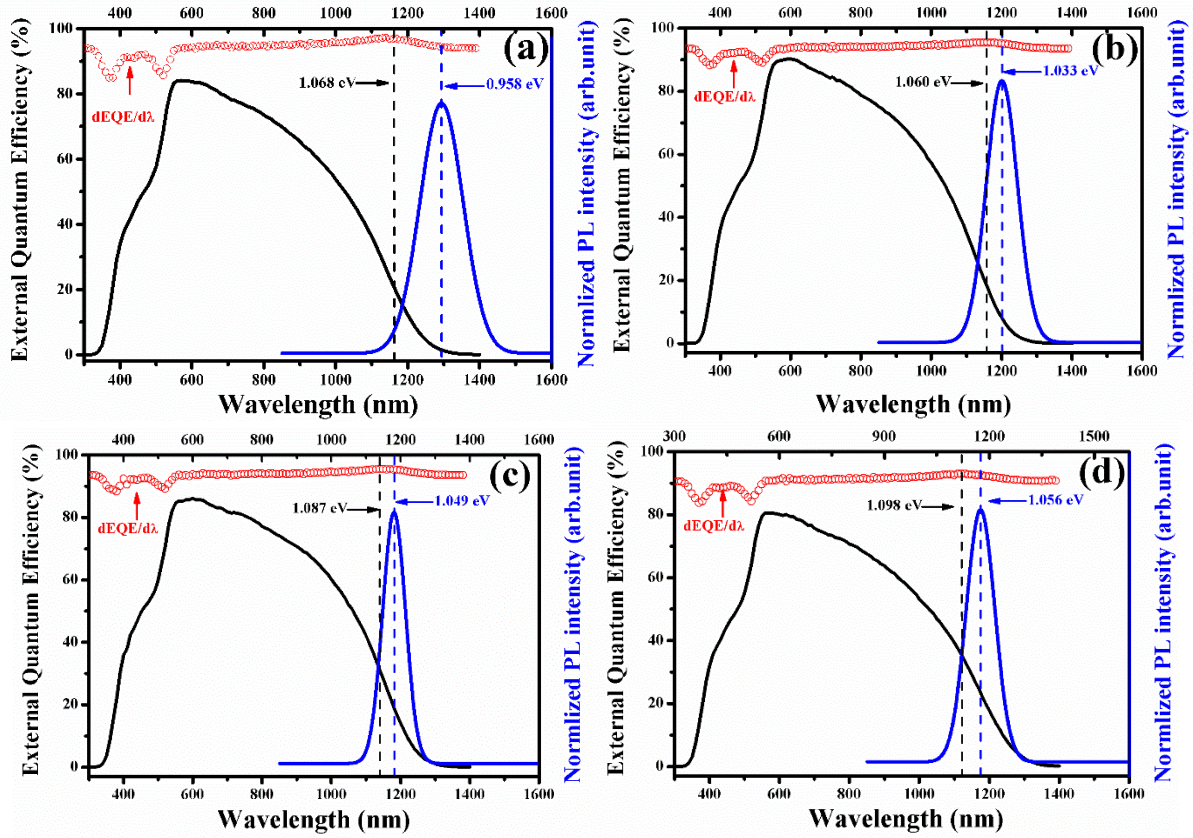

Figure 3. EQE (black), LTPL (blue), and dEQE/dλ (red circles) spectra of CZTSSe TFSCs annealed under the initial chamber pressure of (a) 400, (b) 500, (c) 600, and (d) 700 Torr.

The aforementioned results motivate us to further optimize the fabrication processes of TFSCs based on CZTSSe films annealed under the initial pressure of 500 Torr. The optimization processes include (i) reducing CdS layer thickness, (ii) introducing a MgF_2 anti-reflection layer, and (iii) fine tuning compositional ratio of CZTSSe, as shown in Figure S8. Figure 4 shows (a) *J-V* and (b) EQE curves of the champion CZTSSe device with a PCE of 11.8%, a V_{oc} of 485 mV, a J_{sc} of 37.50 mA/cm^2, and a FF of 64.91%, measured under an AM 1.5G illumination. The result was certified by Korea Institute of Energy Research (KIER), as shown in Figure S9. The EQE spectrum of this device shows nearly 95% in the visible region and then decreases in the longer wavelength region, as shown in Figure 4b. Importantly, the V_{oc}-deficit of this champion device (~582 mV), with a 10 meV energy difference between the bandgaps measured from *d*EQE/*d*λ and LTPL, is among the smallest values for kesterite TFSCs reported in literature.

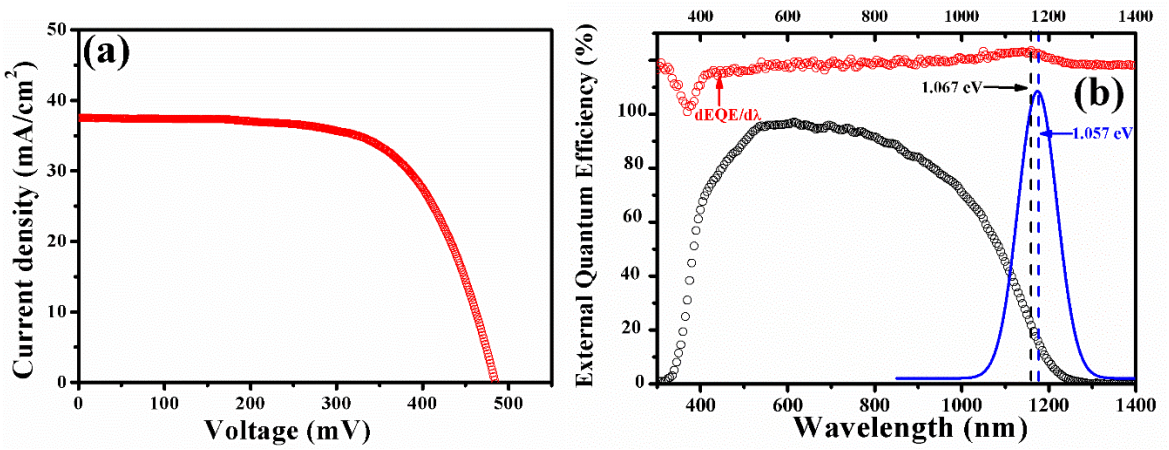

Figure 4. (a) *J-V* curve and (b) EQE (black), LTPL (blue), and dEQE/dλ (red circles) spectra of the champion CZTSSe TFSC.

Though our CZTSSe TFSC shows the smallest value of V_{oc}-deficit and the smallest band tailing measured from *d*EQE/*d*λ and LTPL (10 meV), the device efficiency is still lower than the current world-record CZTSSe TFSC prepared by a hydrazine based on solution process reported by Mitzi et al. at IBM.[2-3] The comparison of our device and the world-record efficiency device is summarized in Table S3. The device parameters are calculated based single diode equations (Equation S1 and S2) using the *J-V* curves, and the calculated graphs are shown in the Figure S10. It is seen that our champion device shows a lower *FF*, which may be due to the higher recombination velocity at the CZTSSe/Mo interface. As shown in Figure 1, our CZTSSe thin films contain rather small grains and voids near the CZTSSe/Mo interface. Consequently, a large density of grain boundaries increases nonradiative recombination. As a result, our champion device shows a higher ideality of 1.75 and a higher dark of 2.5 x 10^{-5} mA/cm^2 than that of the IBM device (1.45 and 7.0 x 10^{-8} mA/cm^2, respectively). Interestingly, however, the V_{oc}-deficit of our CZTSSe TFSC (582 mV) is smaller than that of IBM device (617 mV). This discrepancy can be attributed to the lower bandgap of the present CZTSSe TFSC.

In conclusion, we have studied the impacts of the initial chamber pressure during annealing process on band tailing in CZTSSe thin films and corresponding solar performance. The morphology and crystal structure of CZTSSe thin films were not significantly changed regardless of initial chamber pressure,

however, the device performance of CZTSSe TFSCs was strongly dependent on initial chamber pressure. In particular, the analysis on the *d*EQE/*d*λ and LTPL data revealed that band tail defect densities in CZTSSe films can be controlled by the initial annealing pressure. Using this strategy, we demonstrated the best CZTSSe TFSC with a PCE of 11.8% with a record low V_{oc}-deficit of 582 mV, and a small energy difference of 10 meV between bandgaps measured from *d*EQE/*d*λ and LTPL. This facile process could provide an effective approach for large scale manufacturing of CZTSSe TFSCs.

EXPERIMENTAL METHODS

The Cu-Sn-Zn stacked metallic precursor thin films were deposited on Mo coated soda lime glass substrates using DC sputtering technique at 0 ºC. The precursor thin films were annealed under Ar atmosphere to form the Cu-Zn and Cu-Sn alloys at 300 ºC for 60 min. To synthesize the CZTSSe thin films, the chalcogenide powders such as S and Se and precursor thin films were placed in a graphite box in a closed isothermal chamber system and heated to 520 ºC for 10 min. The annealing chamber including precursor thin film, chalcogenide powder in the graphite box was evacuated to a base pressure of 5.0 x 10^{-3} Torr, and then the initial pressures were controlled as 400, 500, 600, and 700 Torr through adjusting Ar gas flow to the chamber. The TFSCs were fabricated with a multi-layered structure of MgF_2/Al/Al-Ni/AZO/i-ZnO/CdS/CZTSSe/Mo/Glass. The detailed experimental conditions and characterizations are given in the Supporting Information.

ASSOCIATED CONTENT

Temperature and pressure profiles during whole annealing process, preparation of CZTSSe films and fabrication processes of Al/Al-Ni/AZO/i-ZnO/CdS/CZTSSe/Mo/Glass structured solar cells, Raman spectra using different exitation laser sources, TEM image at interface between CZTSSe

and Mo back layer, measured *J-V* curves, –ln(1-EQE) vs. photo energy plots, and certificated champon efficiency, efficieny evolution map through optimizing process, d*J*/d*V* vs. voltage, d*V*/d*J* vs. $(J + J_{sc})^{-1}$, $(J + J_{sc} - GV)$ vs. (*V-RJ*) plots, summarized device parameters.

AUTHOR INFORMATION

ORCID

Seung Wook Shin: 0000-0002-3396-2535

Mahesh P. Suryawanshi: 0000-0003-4711-7655

Uma V. Ghorpade: 0000-0001-8631-7030

Zhaoning Song: 0000-0002-6677-0994

Yanfa Yan: 0000-0003-3977-5789

Jin Hyeok Kim : 0000-0003-4711-7655

E-mail:k2kang1212@nate.com (M.G. Gang), seung.shin@utoledo.edu (S.W. Shin), maheshsuryawanshi@chonnam.ac.kr (M.P. Suryawanshi), umaghorpade@chonnam.ac.kr (U.V. Ghorpade), Jun Sung Jang (jjst115@naver.com), zhaoning.song@utoledo.edu (Z. Song), yunjh92@kier.re.kr (J.H. Yun)

Notes

The authors declare no competing financial interest.

ACKNOWLEDGMENT

This work was supported by the Human Resources Development program (No. 20164030201310) of the Korea Institute of Energy Technology Evaluation and Planning (KETEP) grant funded by the Korea government Ministry of Trade, Industry and Energy and was partially supported by the Technology Development Program to Solve Climate Changes of the National Research Foundation (NRF) funded by the Ministry of Science, ICT & Future Planning (2016936784). Work

at University of Toledo was supported by NSF under contract no ECCS-1665028 and DMR-1534686

TOC GRAPHICS

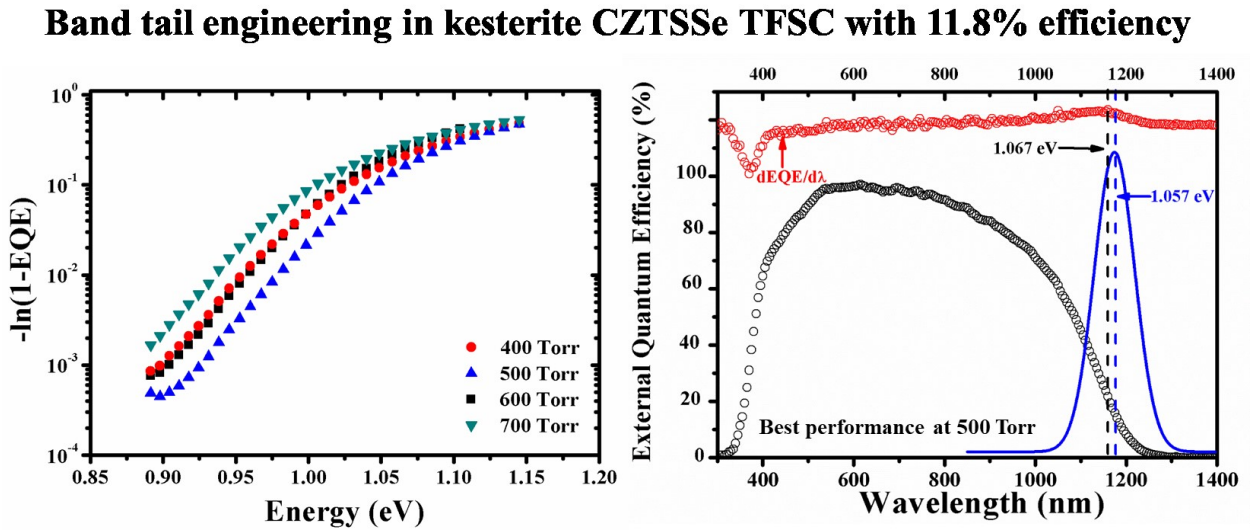

REFERENCES

(1) Hong, C. W.; Shin, S. W.; Suryawanshi, M. P.; Gang, M. G.; Heo, J.; Kim, J. H., Chemically Deposited CdS Buffer/Kesterite Cu_2znsns_4 Solar Cells: Relationship between CdS Thickness and Device Performance. *ACS Appl. Mater. Interfaces* **2017**, *9*, 36733-36744.

(2) Wang, W.; Winkler, M. T.; Gunawan, O.; Gokmen, T.; Todorov, T. K.; Zhu, Y.; Mitzi, D. B., Device Characteristics of CZTSSe Thin-Film Solar Cells with 12.6% Efficiency. *Adv. Energy Mater.* **2014**, *4*, 1301465.

(3) Gang, M. G.; Shin, S. W.; Hong, C. W.; Gurav, K. V.; Gwak, J.; Yun, J. H.; Lee, J. Y.; Kim, J. H., Sputtering Processed Highly Efficient $Cu_2ZnSn(S,Se)_4$ Solar Cells by a Low-Cost, Simple, Environmentally Friendly, and up-Scalable Strategy. *Green Chem.* **2016**, *18*, 700-711.

(4) Pinto, A. H.; Shin, S. W.; Aydil, E. S.; Penn, R. L., Selective Removal of $Cu_{2-X}(S,Se)$ Phases from $Cu_2ZnSn(S,Se)_4$ Thin Films. *Green Chem.* **2016**, *18*, 5814-5821.

(5) Pinto, A. H.; Shin, S. W.; Sharma, A.; Penn, R. L.; Aydil, E. S., Synthesis of $Cu_2(Zn_{1-X}Co_x)SnS_4$ Nanocrystals and Formation of Polycrystalline Thin Films from Their Aqueous Dispersions. *J. Mater. Chem. A* **2018**, *6*, 999-1008.

(6) Suryawanshi, M.; Shin, S. W.; Ghorpade, U.; Song, D.; Hong, C. W.; Han, S.-S.; Heo, J.; Kang, S. H.; Kim, J. H., A Facile and Green Synthesis of Colloidal Cu_2ZnSnS_4 Nanocrystals and Their Application in Highly Efficient Solar Water Splitting. *J. Mater. Chem. A* **2017**, *5*, 4695-4709.

(7) Jackson, P.; Wuerz, R.; Hariskos, D.; Lotter, E.; Witte, W.; Powalla, M., Effects of Heavy Alkali Elements in $Cu(in,Ga)Se_2$ Solar Cells with Efficiencies up to 22.6%. *Phys. Status Sol. (RRL) – Rap. Res. Lett.* **2016**, *10*, 583-586.

(8) Ford, G. M.; Guo, Q.; Agrawal, R.; Hillhouse, H. W., Earth Abundant Element $Cu_2Zn(Sn_{1-X}Ge_x)S_4$ Nanocrystals for Tunable Band Gap Solar Cells: 6.8% Efficient Device Fabrication. *Chem.Mater.* **2011**, *23*, 2626-2629.
(9) Son, D.-H.; Kim, D.-H.; Park, S.-N.; Yang, K.-J.; Nam, D.; Cheong, H.; Kang, J.-K., Growth and Device Characteristics of CZTSSe Thin-Film Solar Cells with 8.03% Efficiency. *Chem. Mater.* **2015**, *27*, 5180-5188.
(10) Haass, S. G.; Andres, C.; Figi, R.; Schreiner, C.; Bürki, M.; Romanyuk, Y. E.; Tiwari, A. N., Complex Interplay between Absorber Composition and Alkali Doping in High-Efficiency Kesterite Solar Cells. *Adv. Energy Mater.* **2018**, *8*, 1701760.
(11) Pundsack, T. J.; Chernomordik, B. D.; Béland, A. E.; Aydil, E. S.; Blank, D. A., Excited-State Dynamics in CZTS Nanocrystals. *J. Phys. Chem. Lett.* **2013**, *4*, 2711-2714.
(12) Shin, D.; Ngaboyamahina, E.; Zhou, Y.; Glass, J. T.; Mitzi, D. B., Synthesis and Characterization of an Earth-Abundant $Cu_2BaSn(S,Se)_4$ Chalcogenide for Photoelectrochemical Cell Application. *J. Phys. Chem. Lett.* **2016**, *7*, 4554-4561.
(13) Thompson, M. J.; Ruberu, T. P. A.; Blakeney, K. J.; Torres, K. V.; Dilsaver, P. S.; Vela, J., Axial Composition Gradients and Phase Segregation Regulate the Aspect Ratio of Cu_2ZnSnS_4 Nanorods. *J. Phys. Chem. Lett.* **2013**, *4*, 3918-3923.
(14) Gokmen, T.; Gunawan, O.; Todorov, T. K.; Mitzi, D. B., Band Tailing and Efficiency Limitation in Kesterite Solar Cells. *Appl. Phys. Lett.* **2013**, *103*, 103506.
(15) Neuschitzer, M.; Marquez, J.; Giraldo, S.; Dimitrievska, M.; Placidi, M.; Forbes, I.; Izquierdo-Roca, V.; Pérez-Rodriguez, A.; Saucedo, E., V_{oc} Boosting and Grain Growth Enhancing Ge-Doping Strategy for $Cu_2ZnSnSe_4$ Photovoltaic Absorbers. *J. Phys. Chem. C* **2016**, *120*, 9661-9670.
(16) Rey, G.; Larramona, G.; Bourdais, S.; Choné, C.; Delatouche, B.; Jacob, A.; Dennler, G.; Siebentritt, S., On the Origin of Band-Tails in Kesterite. *Sol. Energy Mater. Sol. Cells* **2018**, *179*, 142-151.
(17) Xie, H.; López-Marino, S; Olar, T.; Sánchez, Y.; Neuschitzer, M.; Oliva, F.; Giraldo, S.; Izquierdo-Roca, V.; Lauermann. I.; Pérez-Rodríguez, A.; Saucedo. E., Impact of Na Dynamics at the $Cu_2ZnSn(S,Se)_4$/CdS Interface During Post Low Temperature Treatment of Absorbers. *ACS Appl. Materi. Interfaces* **2016**, *8*, 5017-5024.
(18) Rey, G.; Larramona, G.; Bourdais, S.; Choné, C.; Delatouche, B.; Jacob, A.; Dennler, G.; Siebentritt, S., On the Origin of Band-Tails in Kesterite. *Sol. Energy Mater. Sol. Cells* **2018**, *179*, 142-151.
(19) Chen, S.; Yang, J.-H.; Gong, X. G.; Walsh, A.; Wei, S.-H., Intrinsic Point Defects and Complexes in the Quaternary Kesterite Semiconductor Cu_2ZnSnS_4. *Phys. Rev. B* **2010**, *81*, 245204.
(20) Shin, D.; Saparov, B.; Mitzi, D. B., Photovoltaic Materials: Defect Engineering in Multinary Earth-Abundant Chalcogenide Photovoltaic Materials *Adv. Energy Mater.* **2017**, *7*, 1602366
(21) Lopez-Marino, S.; Sánchez, Y.; Espíndola-Rodríguez, M.; Alcobé, X.; Xie, H.; Neuschitzer, M.; Becerril, I.; Giraldo, S.; Dimitrievska, M.; Placidi, M.; Fourdrinier, L. Izquierdo-Roca, V.; Pérez-Rodríguezad, A.; Saucedo, E. Alkali Doping Strategies for Flexible and Light-Weight $Cu_2ZnSnSe_4$ Solar Cells. *J. Mater. Chem. A* **2016**, *4*, 1895-1907.
(22) Tai, K. F.; Fu, D.; Chiam, S. Y.; Huan, C. H. A.; Batabyal, S. K.; Wong, L. H., Antimony Doping in Solution-Processed $Cu_2ZnSn(S,Se)_4$ Solar Cells. *ChemSusChem* **2015**, *8*, 3504-3511.
(23) Kim, I.; Kim, K.; Oh, Y.; Woo, K.; Cao, G.; Jeong, S.; Moon, J., Bandgap-Graded $Cu_2Zn(Sn_{1-X}Ge_x)S_4$ Thin-Film Solar Cells Derived from Metal Chalcogenide Complex Ligand Capped Nanocrystals. *Chem. Mater.* **2014**, *26*, 3957-3965.
(24) Sun, R.; Zhuang, D.; Zhao, M.; Gong, Q.; Scarpulla, M.; Wei, Y.; Ren, G.; Wu, Y., Beyond 11% Efficient $Cu_2ZnSn(Se,S)_4$ Thin Film Solar Cells by Cadmium Alloying. *Sol. Energy Mater. Sol. Cells* **2018**, *174*, 494-498.

(25) Yan, C.; Sun, K.; Huang, J.; Johnston, S.; Liu, F.; Puthen Veettil, B.; Sun, K.; Pu, A.; Zhou, F.; A. Stride, J.; A. Green, M.; Hao, X., Beyond 11% Efficient Sulfide Kesterite $Cu_2(Zn_{1-x}Cd_x)SnS_4$ Solar Cell: Effects of Cadmium Alloying. *ACS Energy Lett.* **2017**, *2*, 930-936.
(26) Li, J.; Wang, D.; Li, X.; Zeng, Y.; Zhang, Y., Cation Substitution in Earth-Abundant Kesterite Photovoltaic Materials. *Adv. Sci.* **2018**, *5*, 1700744.
(27) Tiwari, D.; Koehler, T.; Lin, X.; Harniman, R.; Griffiths, I.; Wang, L.; Cherns, D.; Klenk, R.; Fermin, D. J., Cu_2ZnSnS_4 Thin Films Generated from a Single Solution Based Precursor: The Effect of Na and Sb Doping. *Chem. Mater.* **2016**, *28*, 4991-4997.
(28) Giraldo, S.; Thersleff, T.; Larramona, G.; Neuschitzer, M.; Pistor, P.; Leifer, K.; Pérez-Rodríguez, A.; Moisan, C.; Dennler, G.; Saucedo, E., $Cu_2ZnSnSe_4$ Solar Cells with 10.6% Efficiency through Innovative Absorber Engineering with Ge Superficial Nanolayer. *Prog. Photovolt. Res. Appl.* **2016**, *24*, 1359-1367.
(29) Khadka, D. B.; Kim, S.; Kim, J., Effects of Ge Alloying on Device Characteristics of Kesterite-Based CZTSSe Thin Film Solar Cells. *J. Phys. Chem. C* **2016**, *120*, 4251-4258.
(30) Bag, S.; Gunawan, O.; Gokmen, T.; Zhu, Y.; Mitzi, D. B., Hydrazine-Processed Ge-Substituted Cztse Solar Cells. *Chem. Mater.* **2012**, *24*, 4588-4593.
(31) Fu, J.; Tian, Q.; Zhou, Z.; Kou, D.; Meng, Y.; Zhou, W.; Wu, S., Improving the Performance of Solution-Processed $Cu_2ZnSn(S,Se)_4$ Photovoltaic Materials by Cd^{2+} Substitution. *Chem. Mater.* **2016**, *28*, 5821-5828.
(32) Salomé, P. M. P.; Rodriguez-Alvarez, H.; Sadewasser, S., Incorporation of Alkali Metals in Chalcogenide Solar Cells. *Sol. Energy Mater. Sol. Cells* **2015**, *143*, 9-20.
(33) Yang, Y.; Huang, L.; Pan, D., New Insight of Li-Doped $Cu_2ZnSn(S,Se)_4$ Thin Films: Li-Induced Na Diffusion from Soda Lime Glass by a Cation-Exchange Reaction. *ACS Appl. Mater. Interfaces* **2017**, *9*, 23878-23883.
(34) Nguyen, T. H.; Kawaguchi, T.; Chantana, J.; Minemoto, T.; Harada, T.; Nakanishi, S.; Ikeda, S., Structural and Solar Cell Properties of a Ag-Containing Cu_2ZnSnS_4 Thin Film Derived from Spray Pyrolysis. *ACS Appl. Mater. Interfaces* **2018**, *10*, 5455-5463